RESEARCH ARTICLE | SEPTEMBER 25 2024

Predictive modeling of MRR, TWR, and SR in spark-EDM of Al-4.5Cu–SiC using ANN and GEP

Shantanu Debnath; Binayak Sen ; Nagaraj Patil; Ankit Kedia; Vikasdeep Singh Mann;
A. Johnson Santhosh ; Abhijit Bhowmik

AIP Advances 14, 095225 (2024)
https://doi.org/10.1063/5.0230832

Predictive modeling of MRR, TWR, and SR in spark-EDM of Al-4.5Cu–SiC using ANN and GEP

Cite as: AIP Advances 14, 095225 (2024); doi: 10.1063/5.0230832
Submitted: 26 July 2024 • Accepted: 4 September 2024 •
Published Online: 25 September 2024

Shantanu Debnath,[1] Binayak Sen,[2,3] Nagaraj Patil,[4] Ankit Kedia,[5] Vikasdeep Singh Mann,[6] A. Johnson Santhosh,[7,a)] and Abhijit Bhowmik[8,9]

AFFILIATIONS

[1] Department of Mechanical Engineering, SRKR Engineering College, Bhimavaram, Andhra Pradesh 534204, India
[2] Centre for Computational Modeling, Chennai Institute of Technology, Chennai, Tamil Nadu 600069, India
[3] Department of Mechanical Engineering, Chennai Institute of Technology, Chennai, Tamil Nadu 600069, India
[4] Department of Mechanical Engineering, School of Engineering and Technology, JAIN (Deemed to be University), Bangalore, Karnataka, India
[5] NIMS School of Mechanical and Aerospace Engineering, NIMS University Rajasthan, Jaipur, India
[6] Department of Mechanical Engineering, Chandigarh Engineering College, Chandigarh Group of Colleges, Jhanjeri, Mohali 140307, Punjab, India
[7] Faculty of Mechanical Engineering, Jimma Institute of Technology, Jimma, Ethiopia
[8] Department of Mechanical Engineering, Dream Institute of Technology, Kolkata 700104, India
[9] Centre of Research Impact and Outreach, Chitkara University, Rajpura 140417, Punjab, India

[a)] **Author to whom correspondence should be addressed:** johnson.antony@ju.edu.et

ABSTRACT

In this study, Al-4.5Cu alloy was reinforced with varying weight percentages of SiC particles (2%, 4%, 6%, and 8%) to create metal matrix composites via the stir casting method. The formation of intermetallic compounds was confirmed through energy dispersive spectroscopy and x-ray diffraction analysis. This article compares the performance of Artificial Neural Network (ANN) and Gene Expression Programming (GEP) models in predicting the Metal Removal Rate (MRR), tool wear rate, and surface roughness in the die-sinking electro-discharge machining (EDM) process of the ex-situ developed Al-4.5%Cu–SiC composites. The study considers three machine parameters—pulse on time (TON), pulse off time (TOFF), and current (I)—along with the weight fraction of SiC particles as input variables for the models. Both ANN and GEP models demonstrated high predictive accuracy for the EDM performance metrics, with correlation coefficients (R) ranging from 0.973 68 to 0.980 65 for the ANN model and 0.980 11 to 0.982 59 for the GEP model. Notably, the GEP model exhibited superior predictive capability, as evidenced by its higher correlation coefficients and lower root mean square error, indicating greater effectiveness in predicting the EDM process outcomes than the ANN model.

I. INTRODUCTION

In the contemporary manufacturing landscape, industries are increasingly driven by the need to achieve higher productivity while maintaining superior quality standards. To address these demands, advancements in materials science, innovative equipment, and cutting-edge techniques have become essential. Among these advancements, the focus has shifted toward the development of materials that are not only stronger and lighter but also cost-effective. Metal matrix composites (MMCs), particularly those based on aluminum, have emerged as a significant solution due to their advantageous properties, which make them suitable for a variety of demanding applications.[1–3] These aluminum-based composites are increasingly replacing conventional metallic alloys in fields such as automotive, aerospace, defense, aquatic sports, and restoration, thanks to their excellent strength-to-weight ratios.[4] In addition

to improving material performance, reducing costs and conserving resources are critical for both environmental and economic sustainability. This necessitates the optimization of manufacturing processes, a focus that has spurred significant interest among researchers. Electro Discharge Machining (EDM) is a prominent non-conventional machining process that operates on the principle of thermoelectric erosion. In EDM, material removal occurs through a sequence of high-frequency sparks generated between an electrode and a workpiece, both submerged in a dielectric medium. This process creates a plasma channel due to the continuous bombardment of ions and electrons, generating localized temperatures between 8000 and 12 000 °C, leading to the vaporization and disintegration of material. The absence of direct physical contact between the tool and the workpiece is a key advantage, making EDM particularly effective for machining hard materials and creating complex shapes with high precision.[5–9]

As the field of Artificial Intelligence (AI) continues to evolve, its applications in predicting the performance of non-conventional machining processes have gained prominence. Neural networks, for example, offer numerous advantages, including minimal formal statistical training requirements and the ability to model complex nonlinear relationships between variables. They can uncover intricate interactions between predictors and responses and provide multiple training algorithms for optimization. Notable implementations include the research by Arunabharathi *et al.*,[10] who utilized Artificial Neural Networks (ANNs) for modeling EDM parameters of air-hardened tool steel in deionized water, and Tarng *et al.*,[11] who developed neural network models to estimate various machining parameters such as pulse duration and peak current. Shandilya *et al.*[12] integrated Response Surface Methodology (RSM) with back-propagation ANNs to model the cutting speed of SiC/Al 6061 MMC during wire-cut EDM. Their studies highlight the critical role of EDM parameters influencing machining outcomes. Ganapathy *et al.*[13] compared ANN and RSM models for predicting the Material Removal Rate (MRR) in EDM using EN-8 material. Results showed that RSM outperformed ANNs in forecasting the coefficient of determination (R^2), Root Mean-Square Error (RMSE), and Average Absolute Deviation (AAD). Sreebalaji and Kumar[14] fabricated aluminum metal matrix composites with fly ash particles of varying sizes using stir casting. They machined these composites with EDM and studied the influences of process parameters on the material removal rate (MRR), tool wear rate (TWR), and surface quality (SR). An artificial neural network predicted these outcomes, matching experimental results and providing a valuable technical database for various applications.

Despite the efficacy of neural networks, their black-box nature and reliance on sigmoid activation functions can lead to increased complexity with non-linearity and potential overfitting issues. This computational burden and the experimental nature of ANN model development underscore the need for more efficient methodologies. Gene Expression Programming (GEP) offers a promising alternative, overcoming many limitations associated with traditional AI models. GEP is a population-based evolutionary method that combines the strengths of both genetic algorithms and programming.[15–20] It provides a closed-form analytical expression for parameter analysis and evaluation, offering advantages over classical regression techniques by eliminating the need for predefined fitness functions.[21–26] This study aims to enhance the MRR and minimize the TWR and SR in EDM processes. While conventional AI techniques such as fuzzy logic, ANNs, and ANFISs have made significant contributions to meta-modeling, the application of GEP in manufacturing remains underexplored. Given its advantages in providing explicit relationships between variables with simple and efficient iterations, GEP presents a valuable methodology for modeling EDM process parameters. This study represents a pioneering effort to apply GEP to accurately model and optimize the EDM process, addressing a crucial gap in the current literature and offering potential advancements for the manufacturing industry.

II. EXPERIMENTAL DETAILS

A. Preparation of MMCs

In this study, we aimed to develop low-cost aluminum Metal Matrix Composites (Al-MMCs) using an ex-situ stir casting technique. The matrix material was pure aluminum (99.99%) combined with 4.5 wt. % copper. The ceramic reinforcement utilized was commercial α-type silicon carbide (SiC) particles with a size range of 25 ± 6 μm. Figures 1(a)–1(c) illustrate the Field Emission Scanning Electron Microscopy (FESEM) micrograph and Energy Dispersive Spectroscopy (EDS) pattern of the cenosphere particles. The average size of the SiC particles ranged from 10 to 40 μm, with a density of 3.21 g/cm^3. The stir-casting process was performed using an induction furnace. Aluminum blocks and copper rods were placed in a graphite-coated crucible. The crucible was heated to ~800 °C to melt the aluminum and copper. To enhance the reactivity of the SiC particles, they were preheated at 900 °C for 4 h before being added to the molten metal.[27] This preheating process ensures better integration of the particles into the matrix. The apparatus used in MMC preparation is shown in Figs. 2(a)–2(c).

A graphite stirrer was employed to achieve thorough dispersion of the SiC particles within the liquid aluminum. The silicon carbide particles were varied in weight fractions of 2, 4, 6, and 8 wt. % for this study. The stirring process involved two distinct phases: the primary stirring was conducted when the slurry was in a semi-solid state, and the secondary stirring occurred just before the molten metal was transferred into a rectangular metallic mold. To mitigate porosity defects in the cast material, 0.2 wt. % hexachloroethane (C_6Cl_6) was used as a degasser. The various process parameters utilized in this paper are shown in Table I. This approach aims to enhance the mechanical properties and performance of the Al-MMCs by ensuring uniform distribution of the SiC particles and minimizing casting defects.

B. Experimental details

In this study, machining was conducted using a Sparkonix small die sinker machine (600 × 400 mm) [see Fig. 3(a)] to drill holes with a diameter of 10 mm into the specimen. The composite blocks, cut into rectangular shapes with dimensions of 20 × 20 × 5 mm, were used for the machining operations. The electrical discharge machining process was powered by a 415 V AC supply and utilized kerosene as the dielectric fluid because of its low chemical reactivity with non-ferrous materials. The 10 mm electrolytic copper electrodes used in the study are characterized by properties detailed in Table II. According to Sohani *et al.*,[28] this type of copper electrode

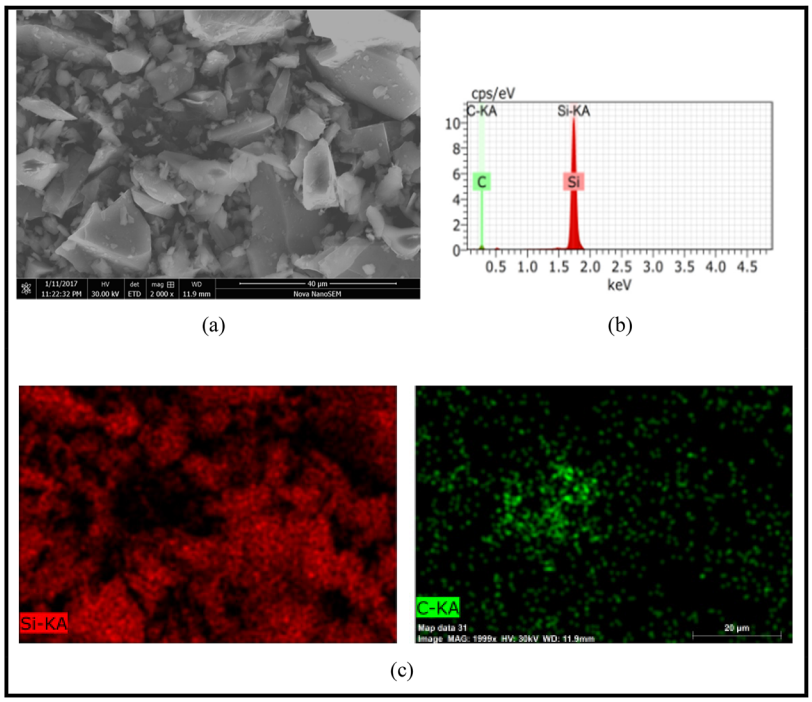

FIG. 1. Electron microscopy of cenosphere particles. (a) SEM. (b) EDS. (c) Surface elemental mapping.

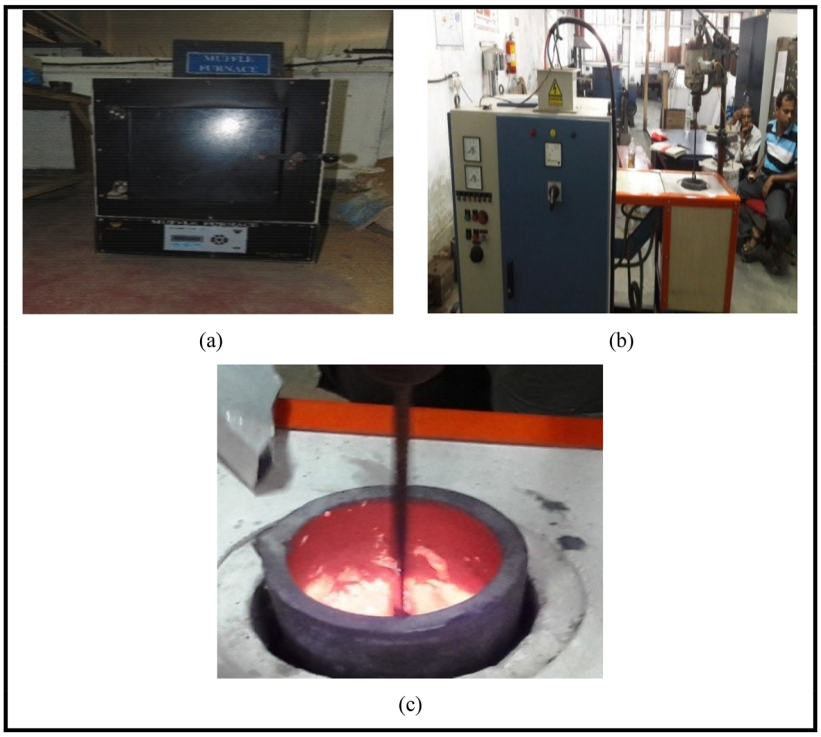

FIG. 2. Preparation of MMC. (a) Muffle furnace used for preheating. (b) Stir casting setup for melting. (c) Liquid hot melt.

TABLE I. Parameters used for the stir-casting process.

Parameters	Value
Spindle speed (rpm)	500
Stirring temperature (°C)	760–780
Stirring time (s)	600
Preheat temperature of SiC (°C)	900
Preheat temperature of mold (°C)	300
Preheat time (min)	90
Powder feed rate (g/s)	1.2–1.6

TABLE II. Properties of electrode material.

Properties	Melting point (°C)	Elastic modulus (E) (N/mm^2)	Poisson's ratio	Density (gm/cm^3)
Value	1083	1.23 × 105	0.26	8.9

TABLE III. The parameter details of the experimental setup.

Working condition	Description
Workpiece	Al–Cu alloys
Electrode	Copper
Dielectric fluid	Kerosene
Discharge current (amps)	6, 9, 12, 15, 18
Pulse on time (T_{on}) (μs)	50, 150, 250, 350, 450

is preferred over others due to its favorable performance characteristics, including a higher MRR and lower TWR when used with an optimal electrode size.

Machining operations were performed for a duration of 2 min per run, with results averaged over three replicates to ensure accuracy. The EDM process generates an electrical potential that creates a spark with significant thermal energy between the electrode and the workpiece. Both the machined specimens [illustrated in Fig. 3(b)] and the electrodes were weighed before and after each machining run using a digital balance with a precision of 0.001 g, enabling precise calculation of the MRR and TWR. Details of the machining conditions are summarized in Table III. The quality of the EDM machining surface is predominantly influenced by machining parameters and the wt. % of reinforcement. The exploratory and operational ranges of these parameters were selected to maintain satisfactory machining surface quality, characterized by minimal heat-affected zones and reduced detritus.[29,30]

To ensure consistency, a uniform gap between the workpiece and electrode surfaces was maintained throughout all trials. Key quality metrics evaluated include the MRR, TWR, and surface roughness. The TWR reflects the loss of electrode material, while surface roughness indicates the machining surface texture. Surface roughness measurements were performed using a Taylor Hobson-80G optical surface roughness tester, with the average center-line roughness (Ra) values recorded for a cut-off length of 0.6 mm. Table IV demonstrates the RSM parametric combinations used in several machining trials, along with the corresponding quality characteristics.

III. PREDICTIVE MODELING TECHNIQUES

A. Artificial neural network

The construction of an ANN is inspired by biological neural systems, particularly the human brain.[31,32] ANNs function as "black box" models, meaning they do not require a comprehensive understanding of the underlying system. Instead, ANNs learn the relationships between input variables and both controlled and uncontrolled variables through the analysis of historical data, akin to the process of nonlinear regression. The architecture of an ANN comprises multiple input neurons connected to neurons in one or more hidden layers. The connections between these neurons are weighted, and these weights determine the network's ability to produce accurate outputs. By adjusting these weights during the training process, ANNs effectively capture complex patterns and relationships within the data.[33–35]

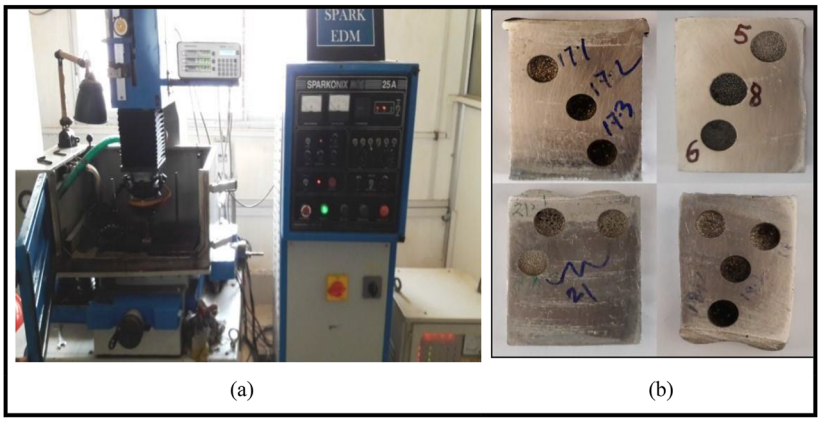

FIG. 3. The electro-discharge machining endeavor. (a) Die sinking EDM. (b) Specimen after EDM.

TABLE IV. Design of experiments and corresponding results.

Expt. No	Weight fraction	Pulse on	Current	Duty cycle	MRR (gm/m)	SR (μm)	TWR (gm/m)
1	−1	−1	−1	−1	0.0239	8.522	0.0084
2	1	−1	−1	−1	0.0153	7.334	0.0033
3	−1	1	−1	−1	0.0452	6.836	0.0041
4	1	1	−1	−1	0.0147	5.846	0.0005
5	−1	−1	1	−1	0.0514	7.296	0.0044
6	1	−1	1	−1	0.0671	6.832	0.0047
7	−1	1	1	−1	0.0554	7.085	0.0026
8	1	1	1	−1	0.0477	6.747	0.0029
9	−1	−1	−1	1	0.052	8.255	0.0032
10	1	−1	−1	1	0.0752	7.513	0.0024
11	−1	1	−1	1	0.0598	6.385	0.0028
12	1	1	−1	1	0.0587	5.607	0.0026
13	−1	−1	1	1	0.0897	7.459	0.0032
14	1	−1	1	1	0.1283	7.699	0.0069
15	−1	1	1	1	0.0698	6.604	0.0041
16	1	1	1	1	0.0975	6.836	0.009
17	−2	0	0	0	0.0551	7.468	0.0052
18	2	0	0	0	0.0693	6.774	0.0055
19	0	−2	0	0	0.0627	7.9035	0.0053
20	0	2	0	0	0.0491	5.994	0.0033
21	0	0	−2	0	0.0089	6.798	0.0011
22	0	0	2	0	0.0757	6.854	0.0044
23	0	0	0	−2	0.0373	7.352	0.0033
24	0	0	0	2	0.1211	7.395	0.0042
25	0	0	0	0	0.0617	7.222	0.0027
26	0	0	0	0	0.0624	7.237	0.0025
27	0	0	0	0	0.0638	7.287	0.0026
28	0	0	0	0	0.0626	7.237	0.0027

The mathematical representation of a particular artificial neuron can be described as follows:

$$y(x) = f\left(\sum_{i=0}^{n} w_i x_i + c\right). \tag{1}$$

Consider a neuron x with n inputs, denoted as x_0, x_1, x_2, …, x_n, and a single output $y(x)$. The weights wi are used to assign values to these inputs, and c represents the bias term. The output of the neuron, after processing through the input and hidden layers with an activation function f, can be expressed as

$$f(x) = \frac{1}{1 + e^{x}}. \tag{2}$$

In the ANN model, the configuration of neurons across the input, hidden, and output layers is determined through iterative trial and error. For the present study, it was found that using 10 neurons in each hidden layer provided the accuracy needed for predicting EDM performance characteristics. The current study employs a multilayer feedforward ANN model to predict output parameters. This model includes multiple neurons in each layer. The network architecture consists of a single input layer, two intermediate hidden layers, and a final output layer. Specifically, the optimal neural network configuration employed in this study is represented as 3-10-10-3, with three neurons in the input layer, ten neurons in each hidden layer, and three neurons in the output layer. The fundamental architecture of the artificial neural network (ANN) is depicted in Fig. 4. For this configuration, a continuously differentiable log-sigmoid activation function was utilized for both the hidden and output neurons. The Mean Squared Error (MSE) was selected as the loss function to be minimized, owing to its advantageous properties of convexity, symmetry, and differentiability, which are conducive to effective optimization. The backpropagation learning algorithm was employed to minimize the MSE in the feedforward network. The model was trained with a dataset comprising 28 experimental values, which resulted in 28 combinations of input and output variables. Details of the network topology, loss functions, and stopping criteria are provided in Table V.

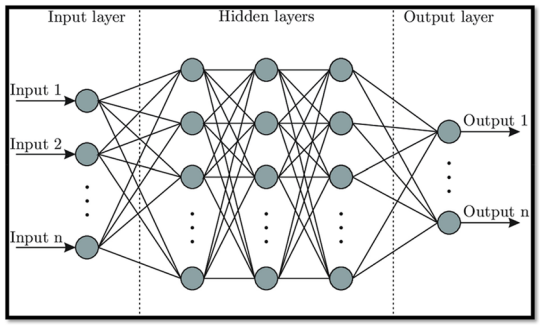

FIG. 4. The basic ANN architecture.

B. Gene expression programming

Ferreira[19] introduced the GEP technique, which is an evolutionary approach that integrates the strengths of both Genetic Algorithms (GAs) and Genetic Programming (GP). GEP represents a robust variant of GP, where input–output relationships are evolved within a tree-based structure. Unlike traditional GP, GEP employs a system where computer programs are optimized through mechanisms inspired by Darwin's theories of replication, mutation, and crossover. In GEP, both simple and linear chromosomes of fixed length are individually encoded and then transformed into parse trees. This approach effectively separates genotype from phenotype, resulting in a significantly faster process—up to 100–10 000 times—than traditional GP.[36–39] Figure 5 illustrates an example of an algebraic tree for a simple expression.

In GEP, a chromosome comprises several genes, each encoded with fixed-length genomes. These genomes generate innovative structures known as expression trees (ETs), which are nonlinear entities exhibiting diverse shapes and sizes.[36] Generally, an individual within genetic programming is represented by a single chromosome, which is segmented into two components: a head and a tail. The length of the tail (t) is a function of the length of the head (h) and the number of arguments in the role (n), as delineated by the following equation:[38]

$$t = h(n - 1) + 1. \tag{3}$$

The head of an expression tree encompasses symbols associated with functions and terminal operators, such as +, −, *, and /. In

TABLE V. Details of ANN topology.

Architecture	Activation function	Training algorithm	Loss function criteria	Stopping criteria
4-10-10-3	Log-sigmoid	Levenberg–Marquardt	Min MSE	Stop the network when validation errors increase

contrast, the tail consists solely of symbols that pertain exclusively to terminal operators. The flowchart for GEP is illustrated in Fig. 6. To determine the optimal solution, the fitness value of the expression trees is the sole criterion for selection. Trees with poor fitness values are discarded, while the remaining population consists of trees selected based on the chosen selection technique.

In this study, GEP was utilized to delineate the relationship between the input and output parameters of EDM. The GEP model was meticulously trained and tested using a dataset comprising SiC weight fraction, pulse on time, current, and duty cycle as input variables, while MRR, TWR, and SR served as output variables. Consistent with the methodology applied in ANNs, 70% of the data were designated for training purposes, with the remaining 30% reserved for validation. The iterative processes of the GEP model were executed using the GeneXproTools software suite.

The construction of the GEP mathematical model incorporated a range of arithmetic operators and mathematical functions from the function and terminal sets, as elaborated in Table VI, to establish the mathematical relationships between the input and output parameters. Each linear chromosome's configuration was determined by the population size, wherein a larger population size necessitated extended iteration times. The program achieved convergence when the model's performance stabilized, indicating no further improvements. The resultant expression trees of the GEP model for the MRR, TWR, and SR are depicted in Figs. 7–9. In these expression trees, d_0, d_1, d_2, and d_3 denote the non-dimensional input values—SiC weight fraction, pulse on time, peak current, and duty cycle, respectively. The optimal explicit equations derived by GEP for the MRR, TWR, and SR are given by Eqs. (4)–(6),

$$\begin{aligned}\mathrm{MRR} = {} & \left(\ln\left(\log\left(\left(\mathrm{d}(0)/\mathrm{c}(1) - (\mathrm{d}(2) + \mathrm{d}(3))\right) + (\mathrm{c}(5) - \mathrm{c}(0))\right)\right)^{1/2}\right)^2 \\ & + \left(\left(\left(\left(\mathrm{c}(0) * \mathrm{d}(1)\right) + (\mathrm{c}(5) * \mathrm{d}(0))\right) * (\mathrm{d}(3) + \mathrm{d}(0))\right) + (\mathrm{c}(2))^3\right)^{1/3}\right)^{1/3} \\ & + \left(\sin\left((\mathrm{c}(3) + \mathrm{d}(2)) + \sin(\mathrm{d}(1))\right)\right)^{1/3} / (1/\sin(\mathrm{c}(5)))^3 \\ & + \ln\left(\left(\left(\left(\exp(\mathrm{d}(3) + \mathrm{d}(3))\right) + (\mathrm{d}(2) * \mathrm{c}(9))\right)^{1/3}\right) + (\mathrm{c}(2))^2\right)^{1/2}\right), \end{aligned} \tag{4}$$

$$\begin{aligned}T\mathrm{WR} = {} & \sin(\mathrm{d}(0) - (\mathrm{d}(0) - (\mathrm{c}(0) + (((\mathrm{d}(2) - \mathrm{d}(1)) + (\mathrm{d}(1) * \mathrm{d}(3))) * \exp(\mathrm{c}9))))) \\ & + \sin\left(\left(\cos\mathrm{d}(0) * 1/\left((\mathrm{c}(9) - \mathrm{d}(2))^2 * ((\mathrm{d}(3) + \mathrm{c}(6)) + \mathrm{d}(1))\right)\right) + \mathrm{c}(1)\right) \\ & + \sin(\mathrm{c}(7)\sin(\sin(\mathrm{d}(2) * \exp(\mathrm{c}(2)) * ((\mathrm{c}(0) * \mathrm{d}(1)) + \mathrm{d}(0))))) \\ & + \sin(\mathrm{c}(0) + ((((\mathrm{d}(0) * \mathrm{d}(3)) - 1/\mathrm{c}(6)) * (\mathrm{d}(0) + \mathrm{d}(0))) * ((\mathrm{d}(0) + \mathrm{d}(2)) * \exp(\mathrm{c}(9))))), \end{aligned} \tag{5}$$

$$\begin{aligned}\mathrm{SR} = {} & \left(\exp\left(((\mathrm{d}(0) - \mathrm{c}(6)) - \mathrm{d}(2)) - \left(\mathrm{d}(0)^2 * \sin(\mathrm{d}(0))\right)\right) + \mathrm{c}(5)\right) \\ & * \left(\left(((((\mathrm{d}(1) - \mathrm{c}(1)) * (\mathrm{d}(2) * \mathrm{d}(1)))/\mathrm{d}(3) - \mathrm{c}(5)) + \mathrm{d}(1))^{1/3}\right) + \mathrm{c}(4)\right) \\ & * (\mathrm{C}(0) - (\mathrm{d}(0) * (\cos(\exp(\sin((1/\mathrm{c}(4)) * (\mathrm{c}(5) - \mathrm{d}(2))))))))) \\ & * (\mathrm{c}(9) + \exp(((\mathrm{d}(2) - \mathrm{c}(3)) - (\mathrm{d}(0) + \mathrm{d}(0))) + ((\mathrm{d}(3) + \mathrm{d}(0)) * \mathrm{d}(3)))). \end{aligned} \tag{6}$$

C. Statistical parameters

The coefficient of determination (R^2), Root Mean Square Error (RMSE), and Mean Absolute Percentage Error (MAPE) are essential metrics for evaluating the predictive accuracy of models such as GEP and ANNs. R^2 indicates the proportion of variance in the dependent variable explained by the model, providing a measure of goodness-of-fit. RMSE quantifies the average magnitude of prediction errors, reflecting how closely the model's predictions match the actual values. MAPE expresses prediction errors as a percentage, offering an intuitive understanding of accuracy. Together, these metrics provide a comprehensive assessment of model performance from different perspectives, ensuring robustness and reliability in predictions.[35,40] Mathematically, R^2, RMSE, and MAPE can be expressed as

$$R^2 = 1 - \frac{\sum_i (N_i - P_i)^2}{\sum_i (P_i)^2}, \tag{7}$$

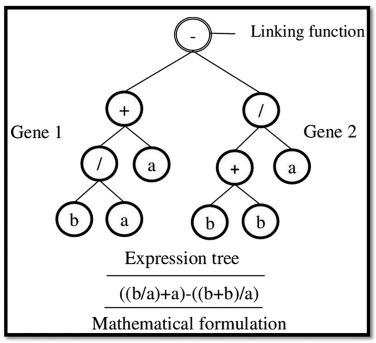

FIG. 5. Example of a GEP expression tree.

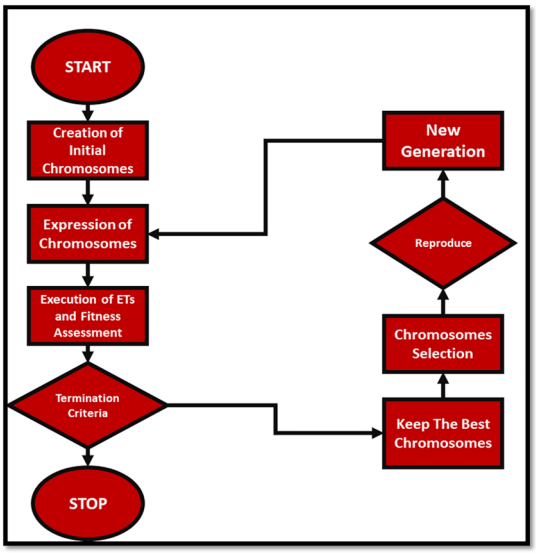

FIG. 6. The flowchart of GEP algorithm.

$$RMSE = \sqrt{\frac{1}{n}\sum_{i}(N_i - P_i)^2}, \tag{8}$$

$$MAPE = \frac{1}{n}\sum_{i}\left|\frac{N_i - P_i}{N_i}\right| \times 100, \tag{9}$$

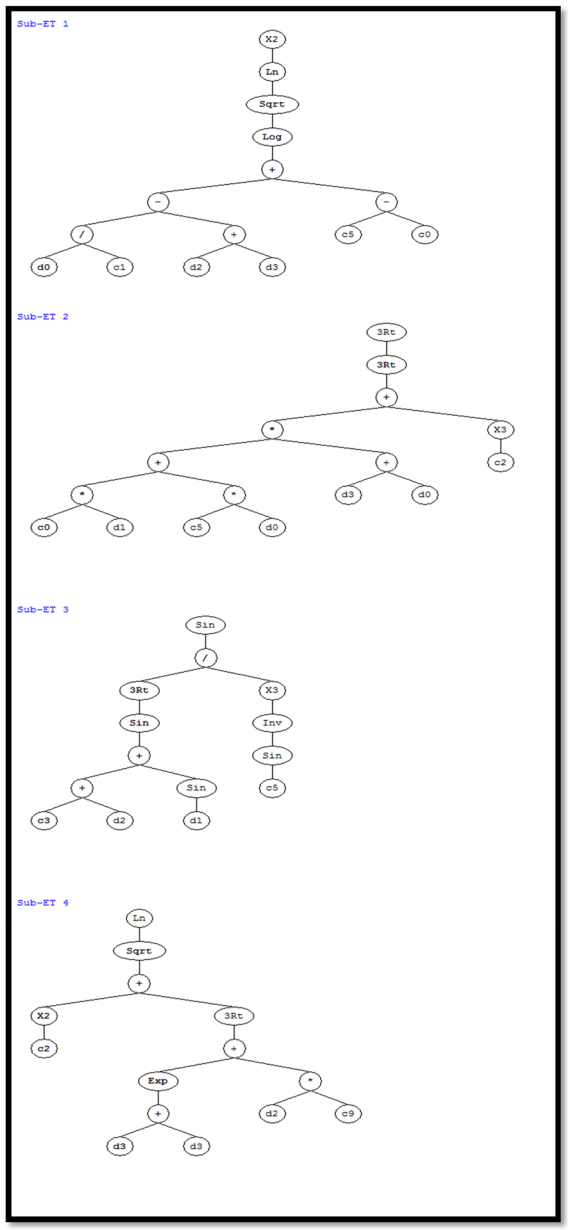

FIG. 7. Expression tree for MRR.

TABLE VI. GEP simulation parameter.

Function set	Chromosome	Head size	No. of genes	Linking function	Mutation rate	Inverse rate	One-point recombination rate	Two-point recombination rate	Gene recombination rate	Gene transportation rate
+, −, *, /, Pow, sqrt, exp, ln(x), log, Inv(1/x), x^2, x^3, cuberoot	30, 40, 50	8, 10, 12	3, 4, 5	Addition	0.044	0.1	0.3	0.3	0.1	0.1

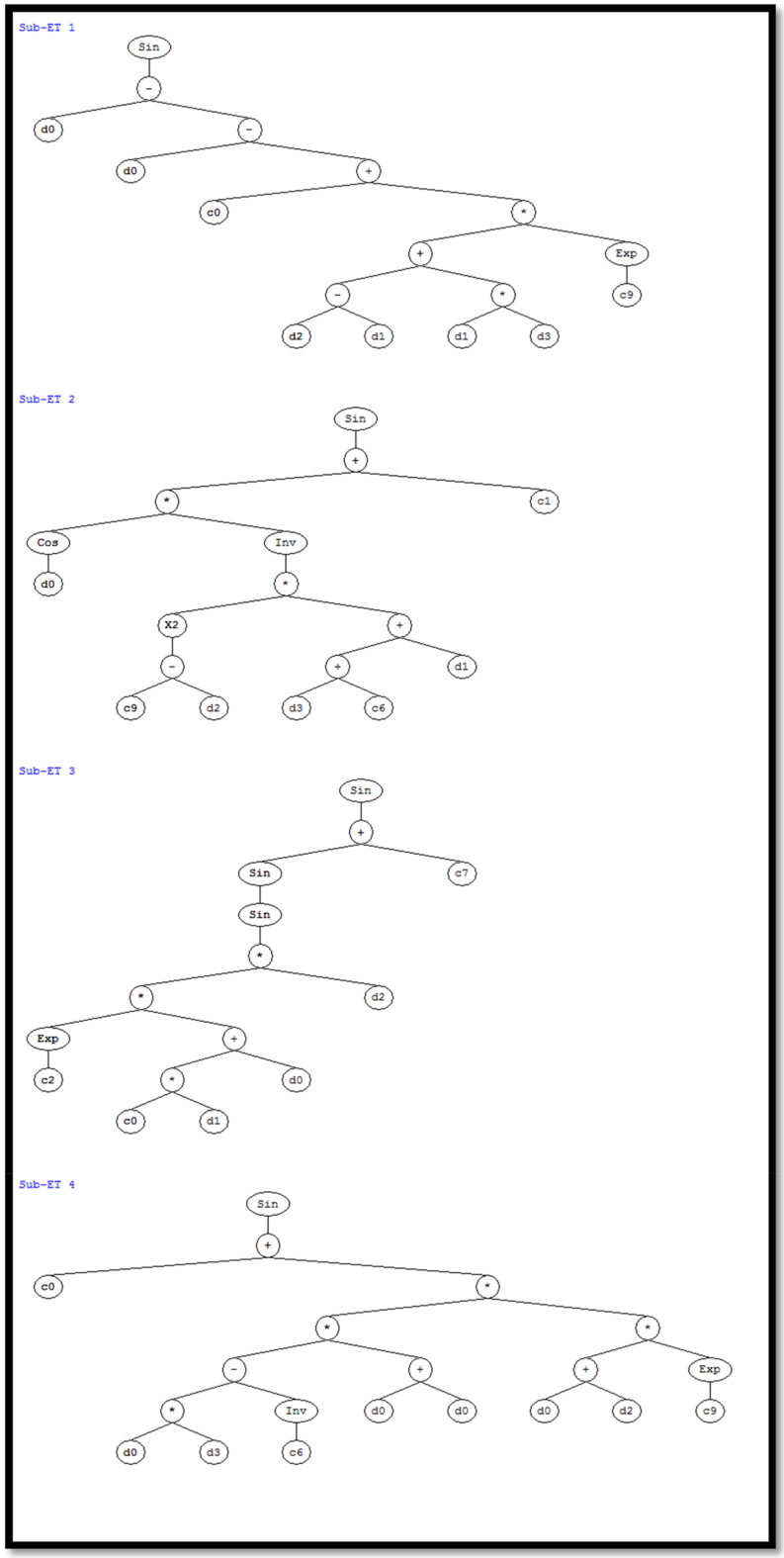

FIG. 8. Expression trees for TWR.

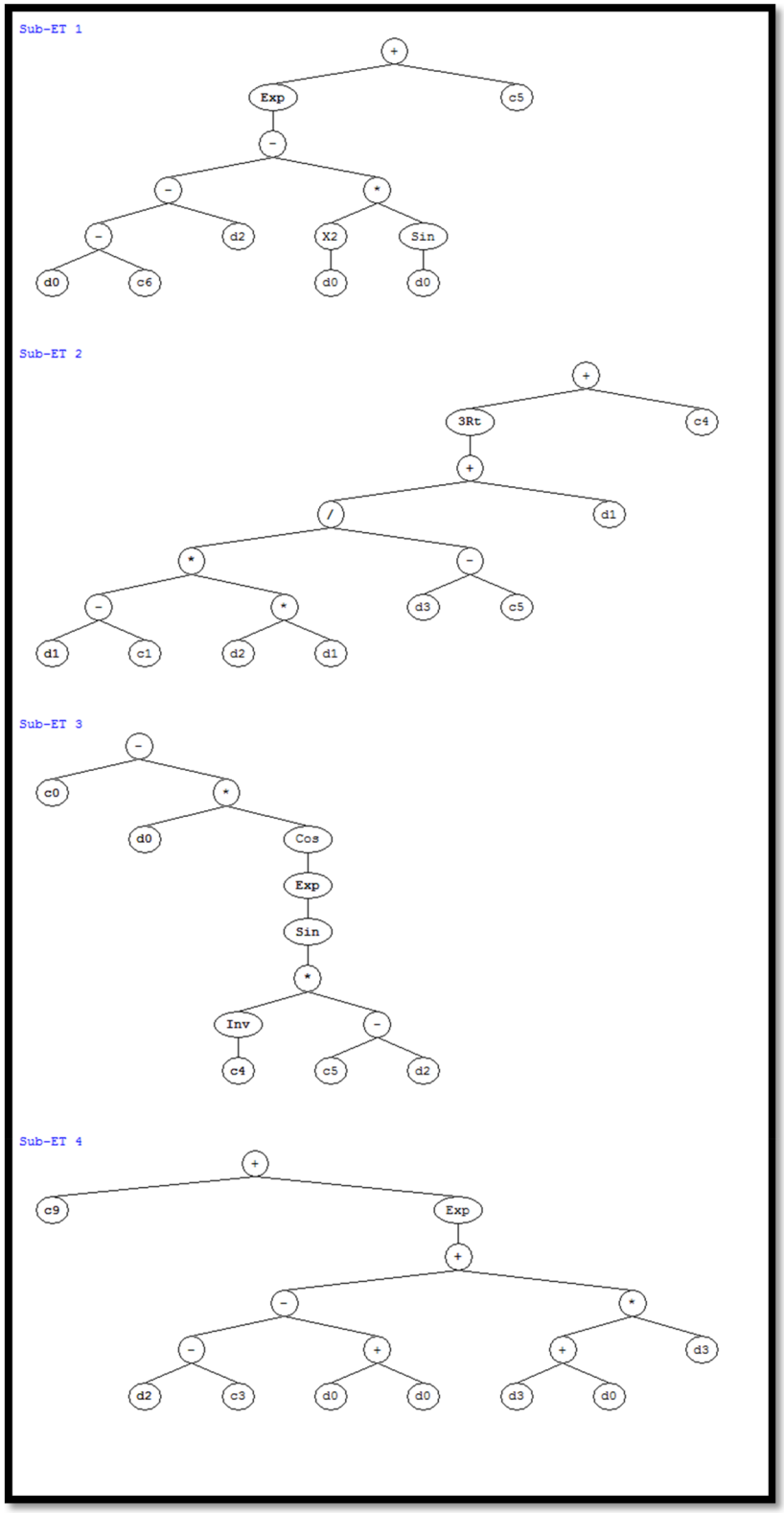

FIG. 9. Expression trees for SR.

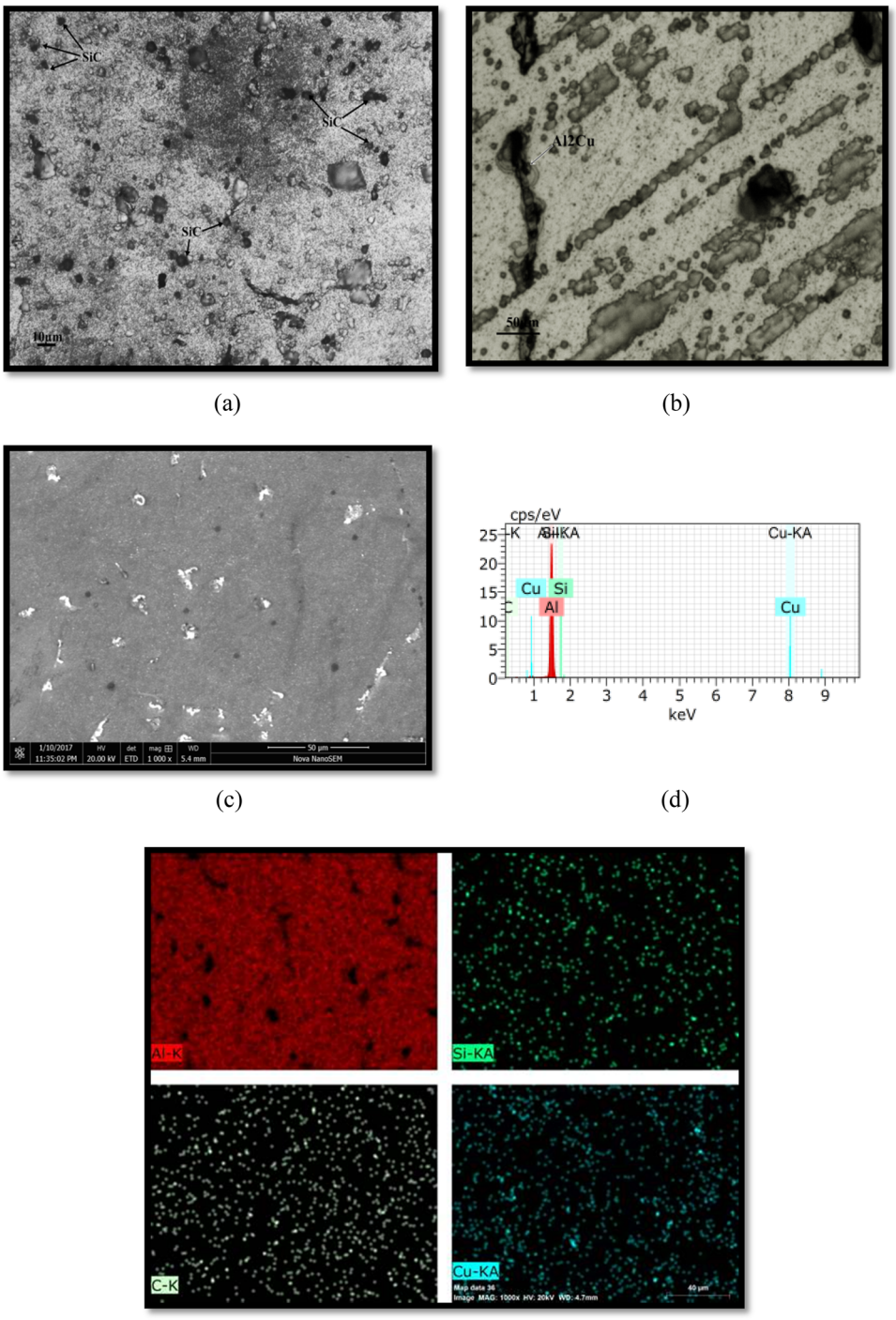

FIG. 10. Characterization of the prepared Al-4.5Cu–SiC composite. (a) Optical micrograph (low resolution). (b) Optical micrograph (high resolution). (c) SEM of Al-4.5Cu–SiC. (d) EDS of Al-4.5Cu–SiC. (e) Surface elemental mapping of Al-4.5Cu–SiC.

where N_i = actual value and P_i = predicted value.

IV. RESULTS AND DISCUSSION

A. Microstructural characterization

Figures 10(a) and 10(b) depict the optical microstructures of cast pure aluminum and Al-4.5%Cu–SiC composites, illustrating the overall structural morphology at low magnification. In these images, the uniform dispersal of SiC particles within the Al–Cu matrix is clearly evident. The volume percentage of primary Al dendritic grains and SiC particles is quantified using graphical point count analysis applied to optical images across 10 frames, equating area percentage to volume percentage based on stereological principles. Furthermore, the average grain size is determined using the intercept method via image analysis software. Interestingly, as the weight fraction of SiC increases, the proportion of dendritic regions decreases, indicating a higher proportion of equiaxed grains and a reduction in overall grain size within the matrix. Concurrently, the matrix accommodates a eutectic mixture of Al and Cu, which favors the precipitation of nanoscale Al_2Cu intermetallics. While these intermetallic phases are challenging to identify under an optical microscope due to their size (few nm), they appear as bright, spheroidal shapes in the SEM image [Fig. 10(c)]. X-ray diffraction (XRD) analysis further confirms the existence of spheroidal Al_2Cu intermetallic phases, which are coherent and act as barriers against crack propagation, thereby enhancing the mechanical properties of the composite material (Fig. 11). In addition, the XRD results indicate that SiC particles remain intact within the matrix without forming detrimental compounds such as Al_4C_3 (aluminum carbide). This preservation of SiC integrity is crucial as it ensures no degradation of the reinforcement phase within the composite.

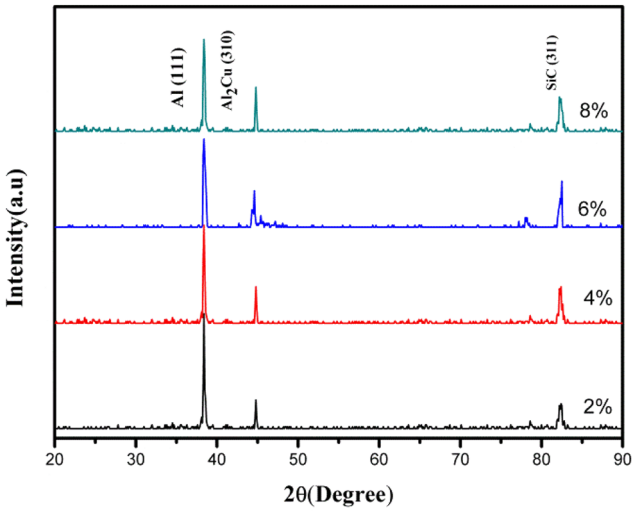

FIG. 11. XRD pattern of the Al-4.5Cu–SiC composite.

B. Prediction of EDM performance characteristics

The prime objective of this numerical investigation is to develop a GEP model for predicting the MRR, TWR, and SR based on experimental data. The input parameters considered are the weight fraction of SiC, pulse duration, peak current, and duty cycle. The GEP model's predictions for the EDM of Al-4.5Cu–SiC composites demonstrated strong correlation statistics, indicating its predictive capability for the MRR, TWR, and SR. Figures 12–14 depict a remarkable alignment between the predicted values and

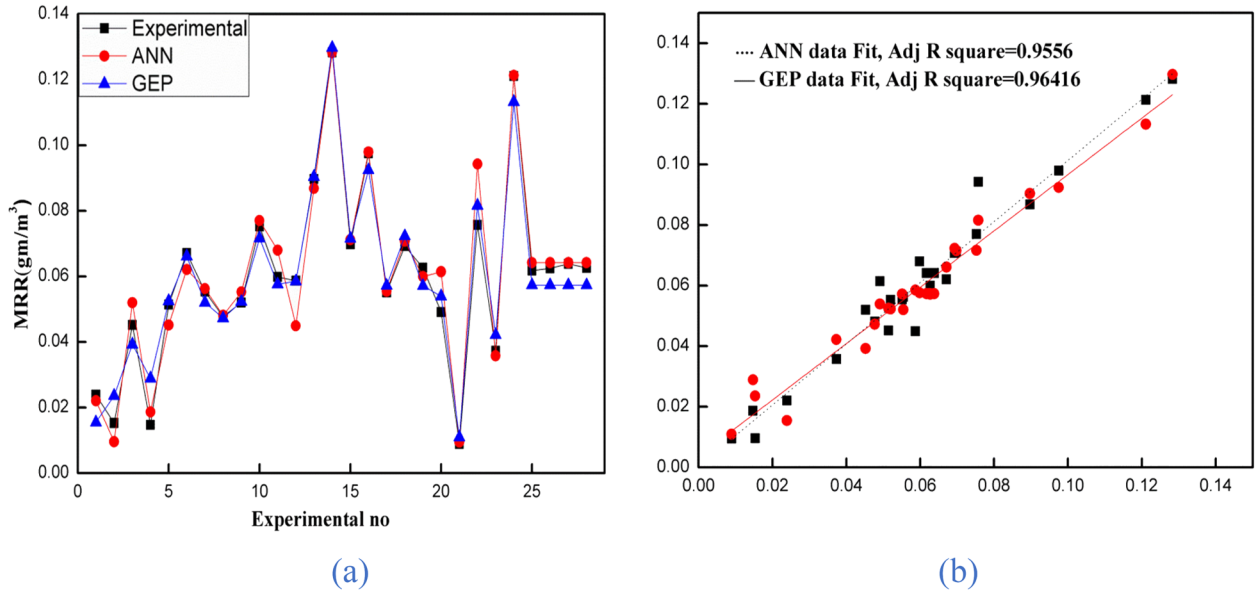

FIG. 12. Comparison of ANN and GEP predicted MRR with experimental data. (a) Prediction deviation. (b) R^2 comparison: ANN vs GEP.

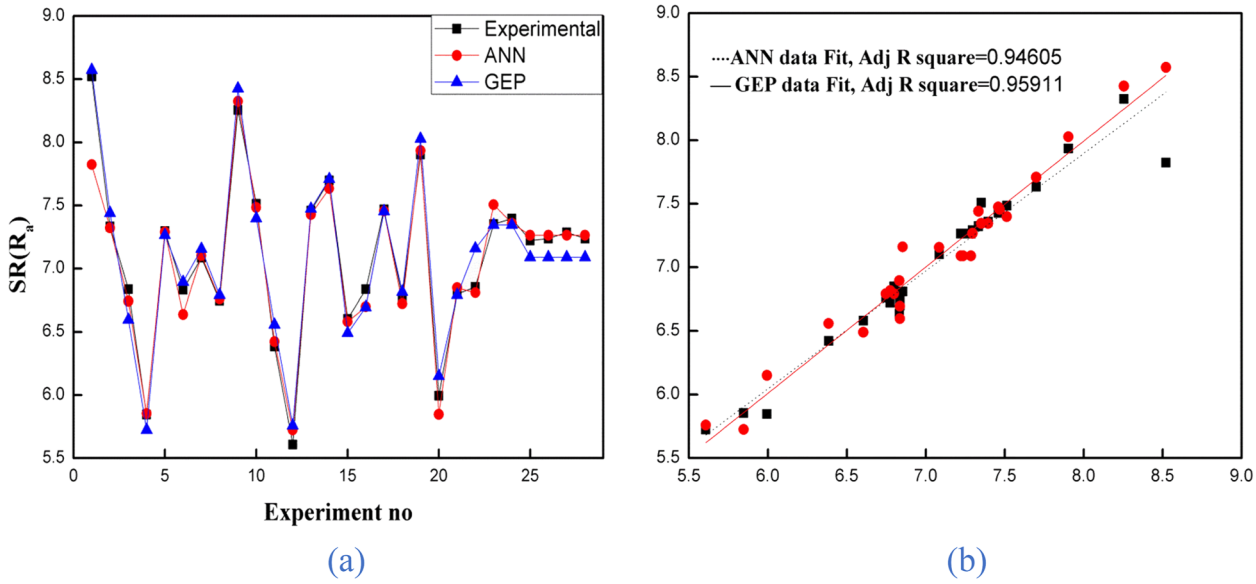

FIG. 13. Comparison of ANN and GEP predicted SR with experimental data. (a) Prediction deviation. (b) R^2 comparison: ANN vs GEP.

experimental observations across the entire data range. This congruence underscores the model's intrinsic sensitivity and robustness, enabling precise plotting of the MRR, TWR, and SR under varying machining operation conditions. In Fig. 12, parts (a) and (b) compare the GEP model predictions with experimental data for the MRR. The GEP model's MRR predictions yielded an R^2 of 0.964 16 and RMSE of 0.005156 gm/min. Similarly, Fig. 13 shows a comparison for the SR, with the GEP model achieving an R^2 value of 0.959 11 and an RMSE of 0.128 758 μm. For the TWR, as shown in Fig. 14, the GEP model attained an R^2 value of 0.9652 and an RMSE of 0.000 050 gm/min.

The comparative performance of the GEP and ANN models is presented in Table VII, using the R_{GEP}/R_{ANN} metric. Data collected from experiments were used for training, testing, and validation, with 70% allocated for training and 15% each for testing and validation. Both studies employed the same training and testing data. Evaluating the results, it can be concluded that the GEP model overtakes the ANN model in predicting EDM responses for the

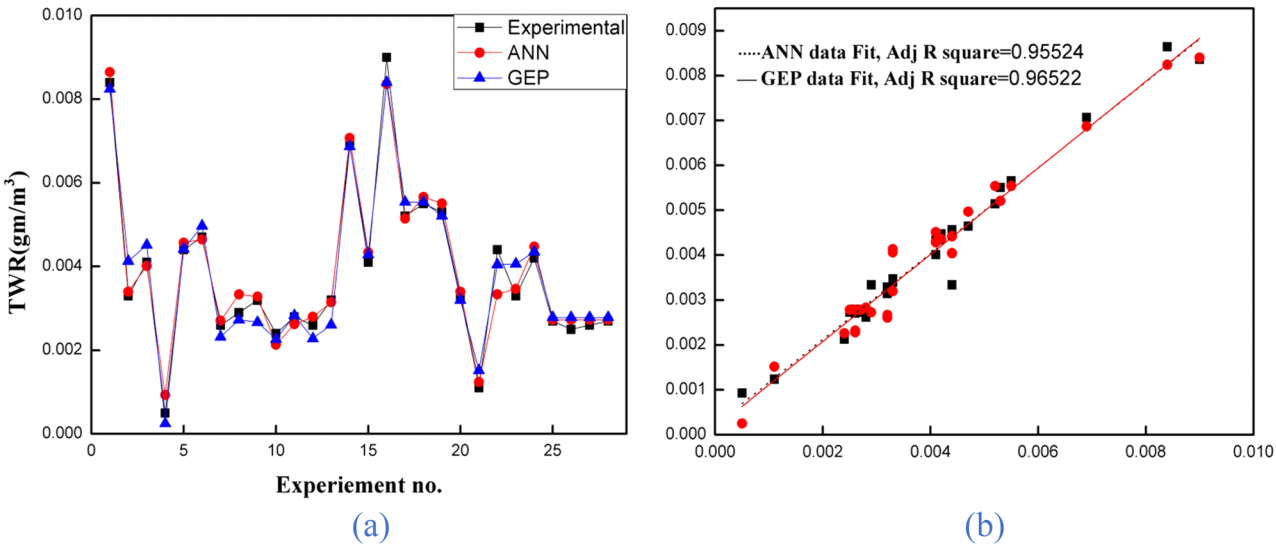

FIG. 14. Comparison of ANN and GEP predicted TWR with experimental data. (a) Prediction deviation. (b) R^2 comparison: ANN vs GEP.

TABLE VII. Comparison of GEP and ANN models.

Parameter	Model	RMSE	Correlation coefficient (R)	MAPE (%)	R_{GEP}/R_{ANN}
MRR(gm/m)	GEP	0.005 156	0.982 59	12.110 159	1.004 152
	ANN	0.005 869	0.978 39	8.520 283	
SR(R_a)	GEP	0.128 758	0.980 112	1.524 038	1.006 605
	ANN	0.151 082	0.973 68	1.076 408	
TWR(gm/m)	GEP	0.000 050	0.982 453	10.176 466	1.001 838
	ANN	0.000 056	0.980 65	8.554 534	

training, testing, validation, and overall datasets. In a similar study, Sen *et al.*[41] employed artificial intelligence-driven meta-models to predict specific cutting energy consumption during machining operations. Their findings revealed that the GEP model outperformed both ANN and RSM models, achieving validation errors ranging from 0.25% to 1.52%.

V. CONCLUSIONS

In conclusion, this study successfully demonstrated the efficacy of GEP as a superior predictive modeling technique compared to the ANN for estimating the MRR, TWR, and SR in the die-sinking EDM process of Al-4.5%Cu–SiC metal matrix composites. The GEP model exhibited higher correlation coefficients and lower RMSE, indicating its enhanced capability in accurately predict EDM performance metrics across various datasets. This advancement underscores the potential of GEP in providing explicit relationships between input and output parameters, thereby facilitating better optimization of machining processes. Furthermore, the study highlights the importance of machine parameters such as pulse on time, pulse off time, and current, along with the weight fraction of SiC particles, in influencing the EDM outcomes. The findings advocate for the integration of GEP in manufacturing processes, particularly in scenarios where traditional AI models may fall short due to their complexity and potential for overfitting. By addressing the limitations of conventional methods, this research paves the way for future explorations into the application of GEP in various manufacturing contexts, ultimately contributing to improved productivity and quality in the industry.

AUTHOR DECLARATIONS

Conflict of Interest

The authors have no conflicts to disclose.

Author Contribution

All authors listed have significantly contributed to the development and the writing of this article.

Shantanu Debnath: Conceptualization (lead); Data curation (lead); Formal analysis (lead); Investigation (lead); Methodology (lead); Software (lead); Validation (lead); Writing – original draft (lead). **Binayak Sen**: Conceptualization (equal); Formal analysis (equal); Methodology (equal); Validation (equal); Writing – original draft (equal); Writing – review & editing (equal). **Nagaraj Patil**: Conceptualization (supporting); Investigation (supporting); Resources (supporting); Writing – review & editing (supporting). **Ankit Kedia**: Formal analysis (supporting); Project administration (supporting); Resources (supporting); Writing – review & editing (supporting). **Vikasdeep Singh Mann**: Formal analysis (supporting); Resources (supporting); Validation (supporting); Writing – review & editing (supporting). **A. Johnson Santhosh**: Data curation (equal); Funding acquisition (equal); Visualization (equal); Writing – review & editing (equal). **Abhijit Bhowmik**: Data curation (supporting); Formal analysis (supporting); Methodology (supporting); Validation (supporting); Writing – review & editing (supporting).

DATA AVAILABILITY

The data that support the findings of this study are available from the corresponding author upon reasonable request.

REFERENCES

[1] S. C. Tjong, "Processing and deformation characteristics of metals reinforced with ceramic nanoparticles," in *Nanocrystalline Materials* (Elsevier, 2014), pp. 269–304.
[2] J. J. Rino, D. Chandramohan, K. S. Sucitharan, and V. D. Jebin, "An overview on development of aluminium metal matrix composites with hybrid reinforcement," Int. J. Sci. Res. **1**(3), 196–203 (2012).
[3] J. Liu, J. Xu, K. W. Paik, P. He, and S. Zhang, "In-situ isothermal aging TEM analysis of a micro Cu/ENIG/Sn solder joint for flexible interconnects," J. Mater. Sci. Technol. **169**, 42–52 (2024).
[4] D. K. Das, P. C. Mishra, S. Singh, and S. Pattanaik, "Fabrication and heat treatment of ceramic-reinforced aluminium matrix composites-a review," Int. J. Mech. Mater. Eng. **9**, 6 (2014).
[5] N. Mohd Abbas, D. G. Solomon, and M. Fuad Bahari, "A review on current research trends in electrical discharge machining (EDM)," Int. J. Mach. Tools Manuf. **47**(7–8), 1214–1228 (2007).
[6] Z. Wang, Y. Yuan, S. Zhang, Y. Lin, and J. Tan, "A multi-state fusion informer integrating transfer learning for metal tube bending early wrinkling prediction," Appl. Soft Comput. **151**, 110991 (2024).
[7] T. Muthuramalingam and B. Mohan, "A review on influence of electrical process parameters in EDM process," Arch. Civ. Mech. Eng. **15**(1), 87–94 (2015).
[8] X. Tian, Y. Zhao, T. Gu, Y. Guo, F. Xu, and H. Hou, "Cooperative effect of strength and ductility processed by thermomechanical treatment for Cu–Al–Ni alloy," Mater. Sci. Eng. A **849**, 143485 (2022).
[9] S. N. Joshi and S. S. Pande, "Development of an intelligent process model for EDM," Int. J. Adv. Des. Manuf. Technol. **45**, 300–317 (2009).
[10] R. Arunbharathi, P. A. Varthanan, and A. G. Danaraj, "Experimental investigation of process parameters in drilling EDM using RSM and ANN in air hardened tool steel (AISI A2)," Asian J. Res. Soc. Sci. Humanit. **7**(1), 96–119 (2017).
[11] Y. S. Tarng, S. C. Ma, and L. K. Chung, "Determination of optimal cutting parameters in wire electrical discharge machining," Int. J. Mach. Tools Manuf. **35**(12), 1693–1701 (1995).
[12] P. Shandilya, P. K. Jain, and N. K. Jain, "Modeling and analysis of surface roughness in WEDC of SiCP/6061 Al MMC through response surface methodology," Int. J. Eng. Sci. Technol. **3**(1), 531–535 (2011).
[13] S. Ganapathy, P. Balasubramanian, B. Vasanth, and S. Thulasiraman, "Comparative investigation of artificial neural network (ANN) and response surface methodology (RSM) expectation in EDM parameters," Mater. Today: Proc. **46**, 9592–9596 (2021).

[14]V. S. Sreebalaji and K. R. Kumar, "Artificial neural networks and multi response optimisation on EDM of aluminium (A380)/fly ash composites," Int. J. Comput. Mater. Sci. Surf. Eng. **6**(3/4), 244–262 (2016).
[15]M. A. Ali Khan, A. Zafar, A. Akbar, M. F. Javed, and A. Mosavi, "Application of Gene Expression Programming (GEP) for the prediction of compressive strength of geopolymer concrete," Materials **14**(5), 1106 (2021).
[16]Y. Chen, S. Sun, T. Zhang, X. Zhou, and S. Li, "Effects of post-weld heat treatment on the microstructure and mechanical properties of laser-welded NiTi/304SS joint with Ni filler," Mater. Sci. Eng. A **771**, 138545 (2020).
[17]A. Nazari and F. Pacheco Torgal, "Modeling the compressive strength of geopolymeric binders by gene expression programming-GEP," Expert Syst. Appl. **40**(14), 5427–5438 (2013).
[18]R. Ji, Q. Zhao, L. Zhao, Y. Liu, H. Jin, L. Wang, L. Wu, and Z. Xu, "Study on high wear resistance surface texture of electrical discharge machining based on a new water-in-oil working fluid," Tribol. Int. **180**, 108218 (2023).
[19]C. Ferreira, "Gene expression programming in problem solving," in *Soft Computing and Industry: Recent Applications* (Springer, London, 2002), pp. 635–653.
[20]C. Yuhua, M. Yuqing, L. Weiwei, and H. Peng, "Investigation of welding crack in micro laser welded NiTiNb shape memory alloy and Ti6Al4V alloy dissimilar metals joints," Opt Laser. Technol. **91**, 197–202 (2017).
[21]A. Ahmad, K. Chaiyasarn, F. Farooq, W. Ahmad, S. Suparp, and F. Aslam, "Compressive strength prediction via gene expression programming (GEP) and artificial neural network (ANN) for concrete containing RCA," Buildings **11**(8), 324 (2021).
[22]Y. Wu, B. Deng, X. Li, Q. Li, T. Ye, S. Xiang, M. C. Zhao, and A. Atrens, "In-situ EBSD study on twinning activity caused by deep cryogenic treatment (DCT) for an as-cast AZ31 Mg alloy," J. Mater. Res. Technol. **30**, 3840–3850 (2024).
[23]B. Sen, S. Debnath, and A. Bhowmik, "Sustainable machining of superalloy in minimum quantity lubrication environment: Leveraging GEP-PSO hybrid optimization algorithm," Int. J. Adv. Des. Manuf. Technol. **130**(9–10), 4575–4601 (2024).
[24]B. Sen, M. Mia, U. K. Mandal, B. Dutta, and S. P. Mondal, "Multi-objective optimization for MQL-assisted end milling operation: An intelligent hybrid strategy combining GEP and NTOPSIS," Neural Comput. Appl. **31**, 8693–8717 (2019).
[25]X. Long, K. Chong, Y. Su, C. Chang, and L. Zhao, "Meso-scale low-cycle fatigue damage of polycrystalline nickel-based alloy by crystal plasticity finite element method," Int. J. Fatigue **175**, 107778 (2023).
[26]H. H. Chu, M. A. Khan, M. Javed, A. Zafar, M. Ijaz Khan, H. Alabduljabbar, and S. Qayyum, "Sustainable use of fly-ash: Use of gene-expression programming (GEP) and multi-expression programming (MEP) for forecasting the compressive strength geopolymer concrete," Ain Shams Eng. J. **12**(4), 3603–3617 (2021).
[27]X. Long, Z. Shen, J. Li, R. Dong, M. Liu, Y. Su, and C. Chen, "Size effect of nickel-based single crystal superalloy revealed by nanoindentation with low strain rates," J. Mater. Res. Technol. **29**, 2437–2447 (2024).
[28]M. S. Sohani, V. N. Gaitonde, B. Siddeswarappa, and A. S. Deshpande, "Investigations into the effect of tool shapes with size factor consideration in sink electrical discharge machining (EDM) process," Int. J. Adv. Des. Manuf. Technol. **45**, 1131–1145 (2009).
[29]R. Adalarasan, M. Santhanakumar, and M. Rajmohan, "Optimization of laser cutting parameters for Al6061/SiCp/Al2O3 composite using grey based response surface methodology (GRSM)," Measurement **73**, 596–606 (2015).
[30]G. Li, W. Chi, W. Wang, X. Liu, H. Tu, and X. Long, "High cycle fatigue behavior of additively manufactured Ti-6Al-4V alloy with HIP treatment at elevated temperatures," Int. J. Fatigue **184**, 108287 (2024).
[31]W. Wu, G. C. Dandy, and H. R. Maier, "Protocol for developing ANN models and its application to the assessment of the quality of the ANN model development process in drinking water quality modelling," Environ. Model. Softw. **54**, 108–127 (2014).
[32]L. Shao, X. Zhang, Y. Chen, L. Zhu, S. Wu, Q. Liu, W. Li, N. Xue, Z. Tu, T. Wang, J. Zhang, S. Dai, X. Shi, and M. Chen, "Why do cracks occur in the weld joint of Ti-22Al-25Nb alloy during post-weld heat treatment?," Front. Mater. **10**, 1135407 (2023).
[33]B. Sen, U. K. Mandal, and S. P. Mondal, "A statistical scrutiny of three prominent machine-learning techniques to forecast machining performance parameters of inconel 690," in *Handbook of Research on Modeling, Analysis, and Application of Nature-Inspired Metaheuristic Algorithms* (IGI Global, 2018), pp. 104–120.
[34]N. Muthukrishnan and J. P. Davim, "Optimization of machining parameters of Al/SiC-MMC with ANOVA and ANN analysis," J. Mater. Process. Technol. **209**(1), 225–232 (2009).
[35]F. Kara, K. Aslantas, and A. Çiçek, "ANN and multiple regression method-based modelling of cutting forces in orthogonal machining of AISI 316L stainless steel," Neural Comput. Appl. **26**, 237–250 (2015).
[36]S. Roy, A. Ghosh, A. K. Das, and R. Banerjee, "Development and validation of a GEP model to predict the performance and exhaust emission parameters of a CRDI assisted single cylinder diesel engine coupled with EGR," Appl. Energy **140**, 52–64 (2015).
[37]S. H. A. Kaboli, A. Fallahpour, J. Selvaraj, and N. A. Rahim, "Long-term electrical energy consumption formulating and forecasting via optimized gene expression programming," Energy **126**, 144–164 (2017).
[38]A. Afradi and A. Ebrahimabadi, "Comparison of artificial neural networks (ANN), support vector machine (SVM) and gene expression programming (GEP) approaches for predicting TBM penetration rate," SN Appl. Sci. **2**, 2004–2016 (2020).
[39]H. Güllü, "Prediction of peak ground acceleration by genetic expression programming and regression: A comparison using likelihood-based measure," Eng. Geol. **141–142**, 92–113 (2012).
[40]H. Xing, J. Zhang, W. Ma, and D. Wen, "Using gene expression programming to discover macroscopic governing equations hidden in the data of molecular simulations," Phys. Fluids **34**(5), 057109 (2022).
[41]B. Sen, A. Bhowmik, C. Prakash, and M. I. Ammarullah, "Prediction of specific cutting energy consumption in eco-benign lubricating environment for biomedical industry applications: Exploring efficacy of GEP, ANN, and RSM models," AIP Adv. **14**(8), 085216 (2024).